Supporting Information

Narrowband ultraviolet-B-emitting LiCaPO$_4$:Gd^{3+} phosphor with super-long persistent luminescence over 100 h

Xihui Shan,[a] Xulong Lv,[a] Dongxun Chen,[a] Yi Zhang,[a] Lixin Ning*[b] and Yanjie Liang*[a]

[a]*Key Laboratory for Liquid-Solid Structure Evolution and Processing of Materials, Ministry of Education, Shandong University, Jinan 250061, P. R. China*
[b]*Anhui Key Laboratory of Optoelectric Materials Science and Technology, Key Laboratory of Functional Molecular Solids, Ministry of Education, Anhui Normal University, 241000 Wuhu, P. R. China*

*Corresponding authors: Yanjie Liang, Lixin Ning
E-mail: yanjie.liang@sdu.edu.cn; ninglx@mail.ahnu.edu.cn

Experimental details

Synthesis

The LiCaPO$_4$:x%Gd^{3+} (x = 0.2, 0.5, 1, 1.5, and 2) NB-UVB persistent phosphors were prepared by the high-temperature solid-state reaction method. Li$_2$CO$_3$ (Aladdin 99.99%), CaCO$_3$ (Macklin 99.99%), NH$_4$H$_2$PO$_4$ (Aladdin 99.99%), and Gd$_2$O$_3$ (Aladdin 99.99%) were used as raw materials. The stoichiometric raw materials were thoroughly ground in an agate mortar and preheated at 600 ℃ in air for 3 h (heating rate, 5 °C min^{-1}). The pre-fired powders were ground again and pressed into 11 mm diameter discs using a 30 T hydraulic press. The disc samples were then sintered at 850 ℃ in air for 6 h (heating rate, 5 °C min^{-1}) to form the solid ceramic discs.

Characterization

The crystal structure and phase composition were checked by using a PANalytical X'Pert PRO powder X-ray diffractometer with Cu Kα_1 radiation (λ = 1.5406 Å). The photoluminescence excitation and emission spectra and persistent luminescence spectra were collected using an Edinburgh FLS1000 fluorescence spectrophotometer equipped with a 450 W xenon arc lamp and a photomultiplier tube (measurement range, 200–900 nm). An 12 W Moxtek MAGPRO X-ray source with tungsten as the anode was used as the excitation source. To charge the LiCaPO$_4$:Gd^{3+} phosphors, an 11 mm diameter phosphor disc was placed at a distance of 1 cm from the X-ray tube, which was operated at 60 kV and 100 μA (dose rate of irradiation is 290.30 mGy/s and the irradiated area is about 2 cm^2 at the position of the phosphor disc.). Thermoluminescence spectra were recorded using an SL18 thermoluminescence setup (Guangzhou Rongfan Science and

Technology Co., Ltd; heating rate, 4 °C s^{-1}). The persistent luminescence emission power intensities were obtained with a Newport 1936-R optical power meter and a Newport 918D-UV-OD3R UV-enhanced silicon photodetector. NB-UVB afterglow images from the persistent phosphors were taken by using an Ofil Scalar UVB camera, which superimposes the NB-UVB images onto the visible images and shows the invisible NB-UVB signal as an area of violet color. UV-VIS spectrophotometer (Shimadzu 2600i) was carried out to measure the diffuse reflectance spectra. The visible images were obtained by a Canon EOS-800D camera.

Computational methodology

The atomic structures of the supercells were fully optimized by periodic DFT using a hybrid exchange–correlation functional in the PBE0[1] scheme (with 30% HF exchange[2]), as implemented in the VASP package.[3,4] The optimizations were carried by minimizing the total energy and Hellmann-Feynman forces to convergence of 10^{-4} eV and 0.02 eV Å^{-1}, respectively. The Li(2s^1), Ca(3p^{6}4s^2), Al(3s^{2}3p^1), P(3s^{2}3p^3), and O(2s^{2}2p^4) were treated as valence electrons, and their interactions with the respective cores were described by the projected augmented wave (PAW) method.[5] Due to the large size of the systems and the high computational cost of hybrid DFT, one k-point Γ was used to sample the Brillouin zone, and the cutoff energy for the plane wave basis was set to 420 eV.

The formation energy of a defect in charge state q was calculated using a standard formalism,[6]

$$\Delta E_{\mathrm{f}} = E_{\mathrm{tot}}(\text{defective}) - E_{\mathrm{tot}}(\text{perfect}) + \Sigma_A \Delta n_A \mu_A + q(\varepsilon_{\mathrm{VBM}} + E_{\mathrm{F}})$$

where E_{tot} is the total energy of the defective or perfect unit cell. Δn_A is the number of

the species A removed from the perfect supercell, and μ_A is the corresponding atomic chemical potential. E_F is the Fermi level measured from the valence band maximum (ε_{VBM}), which was aligned with that of the perfect cell by the macroscopic averaging approach.[7] The correction to the total energy of charged supercells due to finite-cell size was considered by using the method proposed in ref 8. The defect formation energy depends on the chemical potentials of the constituent atoms. In the thermodynamic equilibrium, the chemical potentials are constrained within the following relation

$$\mu_{Li} + \mu_{Ca} + \mu_P + 4\mu_O = \mu_{LiCaPO_4}$$

where μ_{LiCaPO_4} is the total energy of one formula unit of LiCaPO$_4$. Since the materials were synthesized in air (i.e., O-rich atmosphere), μ_O was first approximated by half the energy of O$_2$ plus the effect of temperature and pressure. The atomic chemical potentials of the other species were further determined by thermodynamic equilibrium conditions of various secondary phases containing the species. Three limiting cases (Li-, Ca-, P-poor cases) were considered, and the derived μ_A values therefrom were used to calculate defect formation energies ΔE_f, which represents the lower/upper limits for a point defect at a given Fermi-level under O-rich condition.

Li-poor case

$$\mu_{Ca} = \mu_{CaO} - \mu_O$$

$$\mu_P = 1/2(\mu_{P_2O_5} - 5\mu_O)$$

$$\mu_{Li} = \mu_{LiCaPO_4} - \mu_{Ca} - \mu_P - 4\mu_O$$

Ca-poor case

$$\mu_{Li} = 1/2(\mu_{Li_2O} - \mu_O)$$

$$\mu_P = 1/2(\mu_{P_2O_5} - 5\mu_O)$$

$$\mu_{Ca} = \mu_{LiCaPO_4} - \mu_{Li} - \mu_P - 4\mu_O$$

P-poor case

$$\mu_{\text{Li}} = 1/2\left(\mu_{\text{Li}_2\text{O}} - \mu_{\text{O}}\right)$$

$$\mu_{\text{Ca}} = \mu_{\text{CaO}} - \mu_{\text{O}}$$

$$\mu_{\text{P}} = \mu_{\text{LiCaPO}_4} - \mu_{\text{Li}} - \mu_{\text{Ca}} - 4\mu_{\text{O}}$$

The total energies of the bulk materials Li_2O, CaO, and P_2O_5 were calculated to determine the relevant chemical potentials.

The thermodynamic charge transition levels (or defect levels) correspond to the Fermi-level position at which a transition occurs from one charge state (q) to another (q'). The level position $\varepsilon(q/q')$ with reference to the host VBM were calculated by

$$\varepsilon(q/q') = \frac{\Delta E_f(q'; E_F=0) - \Delta E_f(q; E_F=0)}{q - q'}$$

where ΔE_f (q or q'; $E_F = 0$) are the formation energies of the defect in charge state q or q' when the Fermi level was set at 0 eV.

The defect-trapped exciton (DFT) emission/absorption energies ($\Delta E_{\text{em/ab}}$) were calculated by

$$\Delta E_{\text{em/ab}} = E_{\text{tot}}(D^{q+1}) + \varepsilon_{\text{CBM}} - E_b - E_{\text{tot}}(D^q)$$

where $E_{\text{tot}}(D^{q+1})$ and $E_{\text{tot}}(D^q)$ are the total energies of the supercell containing a defect (D) in the $q+1$ and q charge states, both at the equilibrium structure of the $q+1$ (or q) state for the emission (or absorption) process. ε_{CBM} denotes the energy in the conduction band minimum (CBM), and E_b is the electron−hole binding energy in the excitonic state.

References

1. J. P. Perdew, M. Ernzerhof and K. Burke, Rationale for mixing exact exchange with density functional approximations, *J. Chem. Phys.*, 1996, **105**, 9982–9985.

2. L. Ning, X. Ji, Y. Dong, W. Jin, Y. Huang, Z. Pan and P. A. Tanner, First-principles

study of Ce-doped $Y_3Al_5O_{12}$ with Si–N incorporation: electronic structures and optical properties, *J. Mater. Chem. C*, 2016, **4**, 5214–5221.

3. G. Kresse and J. Furthmüller, Efficient iterative schemes for ab initio total-energy calculations using a plane-wave basis set, *Phys. Rev. B*, 1996, **54**, 11169–11186.

4. G. Kresse and D. Joubert, From ultrasoft pseudopotentials to the projector augmented-wave method, *Phys. Rev. B*, 1999, **59**, 1758–1775.

5. P. E. Blöchl, Projector augmented-wave method, *Phys. Rev. B*, 1994, **50**, 17953–17979.

6. C. Freysoldt, B. Grabowski, T. Hickel, J. Neugebauer, G. Kresse, A. Janotti and C. G. Van de Walle, First-principles calculations for point defects in solids, *Rev. Mod. Phys.*, 2014, **86**, 253–305.

7. T. Mattila and A. Zunger, Deep electronic gap levels induced by isovalent P and As impurities in GaN, *Phys. Rev. B*, 1998, **58**, 1367–1373.

8. G. Makov and M. C. Payne, Periodic boundary conditions in ab initio calculations, *Phys. Rev. B*, 1995, **51**, 4014–4022.
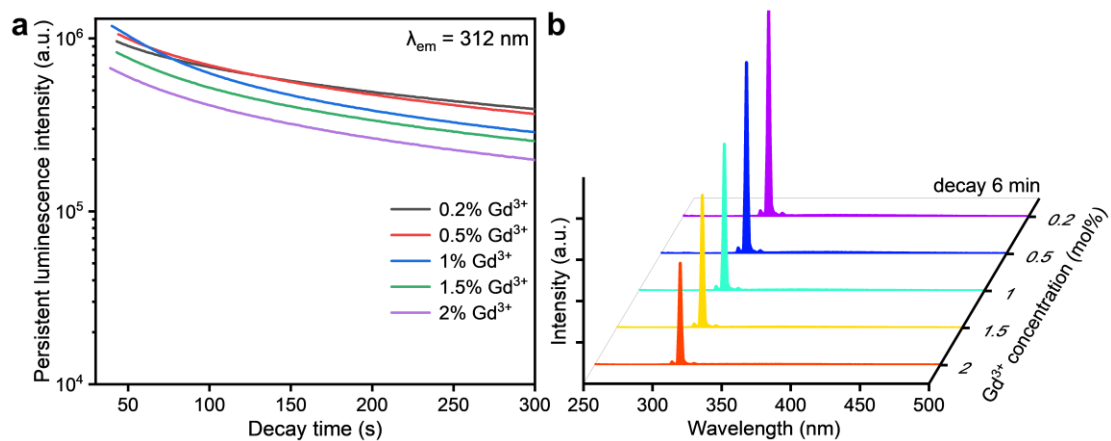
Fig. S1 (a) Concentration-dependent NB-UVB persistent luminescence decay curves of the LiCaPO$_4$:x%Gd^{3+} (x = 0.2, 0.5, 1, 1.5, and 2) phosphors monitored at 312 nm in dark after irradiation by an X-ray beam. (b) Concentration-dependent persistent luminescence emission spectra recorded at 6 min decay after the stoppage of X-ray irradiation.
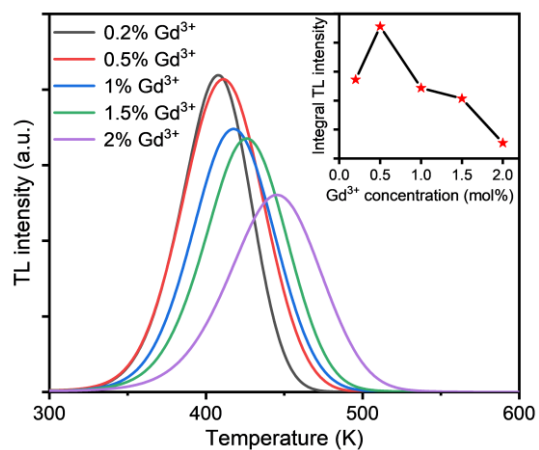
Fig. S2 Thermoluminescence (TL) curves of the $LiCaPO_4$:x%Gd^{3+} ($x = 0.2, 0.5, 1, 1.5,$ and 2) phosphors after irradiation with an X-ray tube for 5 min. TL curves were acquired after 1 min decay by monitoring at 312 nm. The inset shows the integral TL intensities of the $LiCaPO_4$:x%Gd^{3+} phosphors.
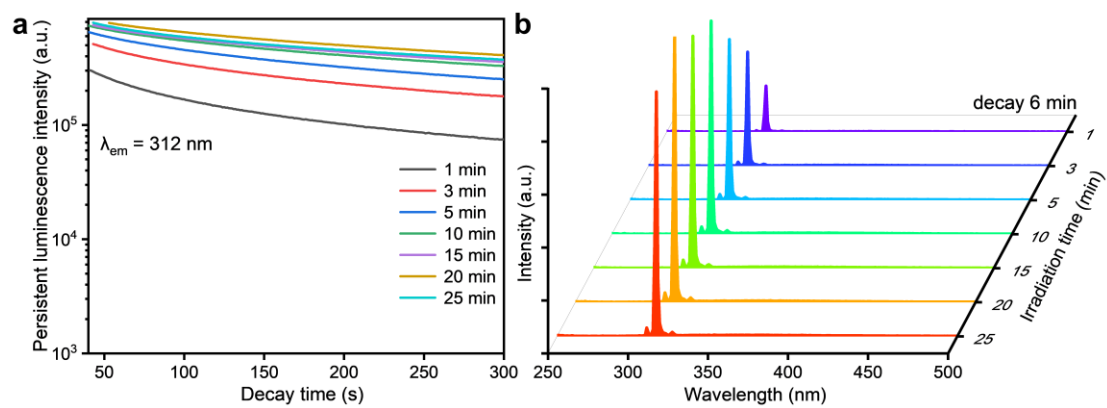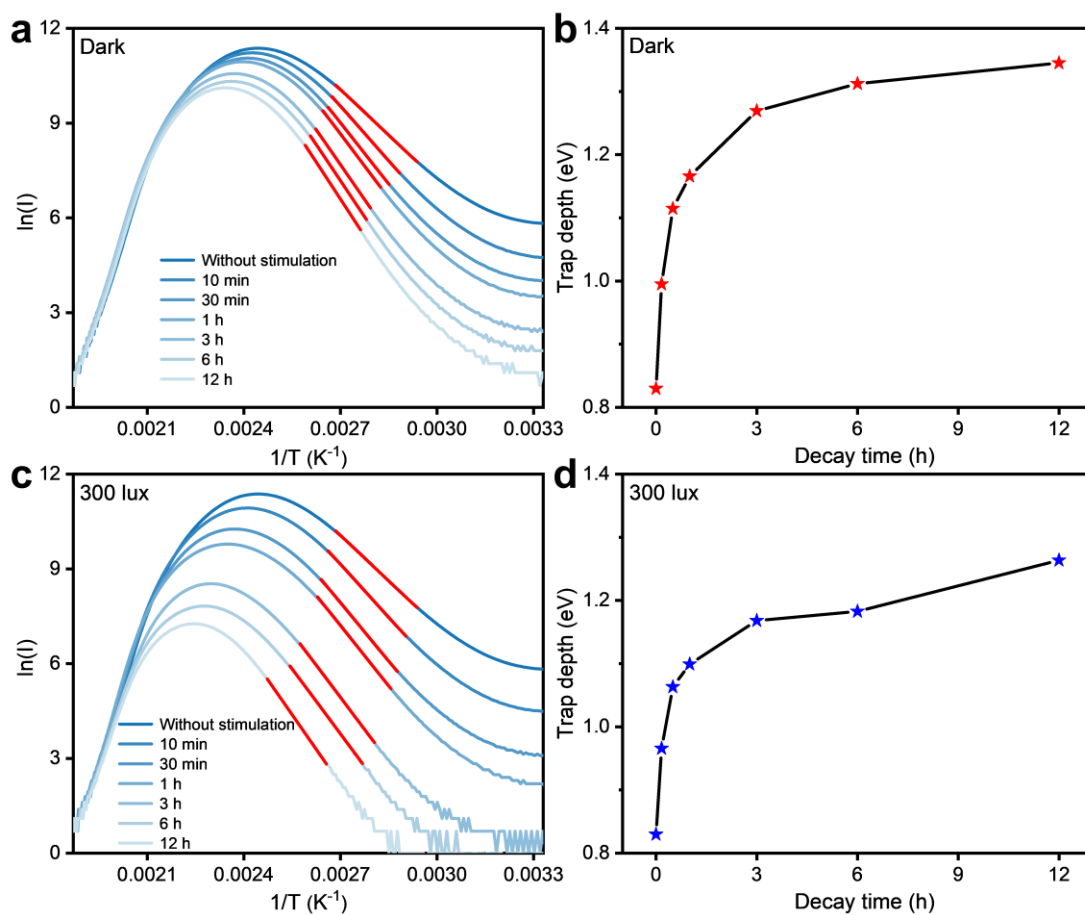
Fig. S3 (a) NB-UVB persistent luminescence decay curves of the LiCaPO₄:0.5%Gd³⁺ phosphor monitored at 312 nm in dark by varying the X-ray irradiation time. (b) Persistent luminescence emission spectra recorded at 6 min decay after the stoppage of X-ray irradiation.
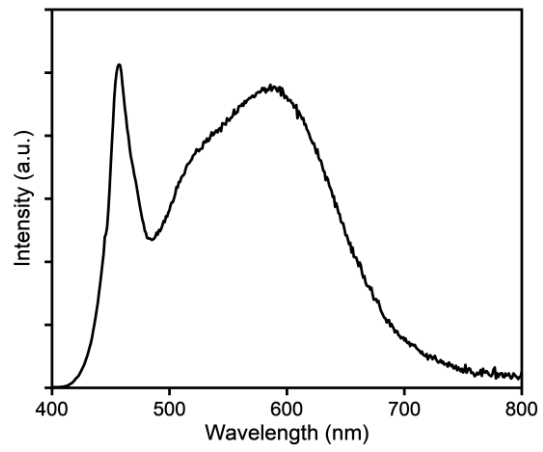
Fig. S4 Emission spectrum of the white LED light source in this work.

Fig. S5 (a,c) Initial rising analysis for the TL curves of the LiCaPO$_4$:0.5%Gd^{3+} phosphor at different decay instants in dark and bright (300 lux) indoor environments after irradiation with an X-ray tube for 20 min. (b,d) The depth of the shallowest occupied trap for each curve was estimated according to the slope of the fitting red straight line.
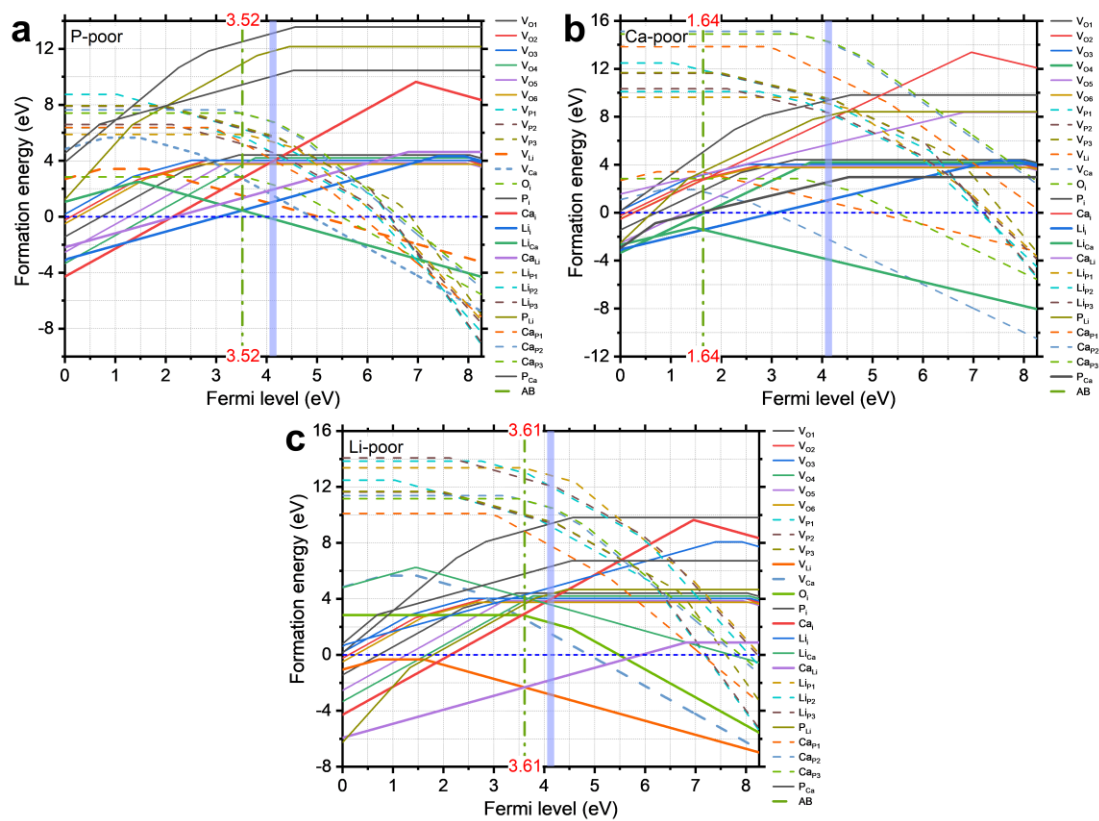
Fig. S6 Calculated formation energies of intrinsic point defects in LiCaPO₄. The Fermi-level positions were determined by the charge-neutrality condition of the defects.
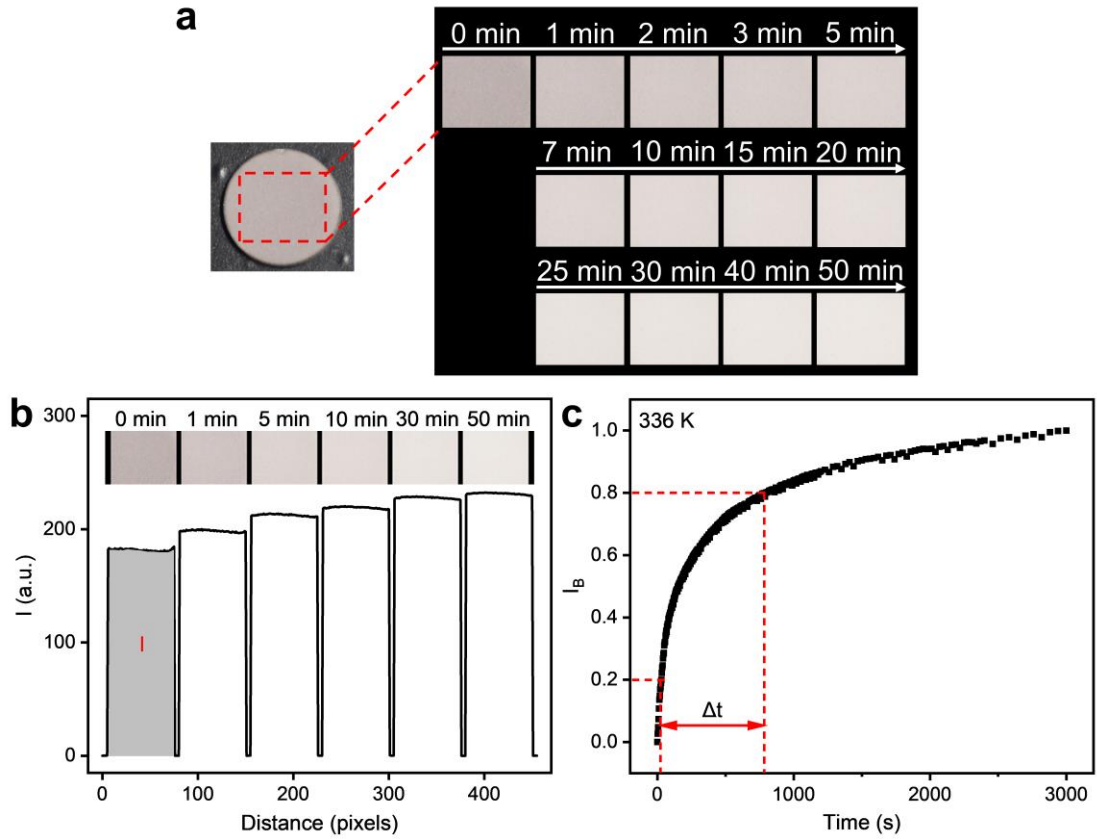
Fig. S7 The decoloration process of the pre-irradiated LiCaPO$_4$:0.5%Gd^{3+} phosphor disc at 336 K was exemplified for brightness extraction. (a) The photograph of the LiCaPO$_4$:0.5%Gd^{3+} phosphor disc immediately after irradiation with an X-ray tube for 20 min and the region of interest (ROI) was intercepted from the raw image and ROI of the decoloration process was arranged with time elapse, where the corresponding brightness value of the whole ROI was extracted through *Image J* software as shown in (b). The normalized brightness value (I_B) was obtained as depicted in (c), where Δt is the interval of time during which the brightness increased from 0.2 to 0.8.
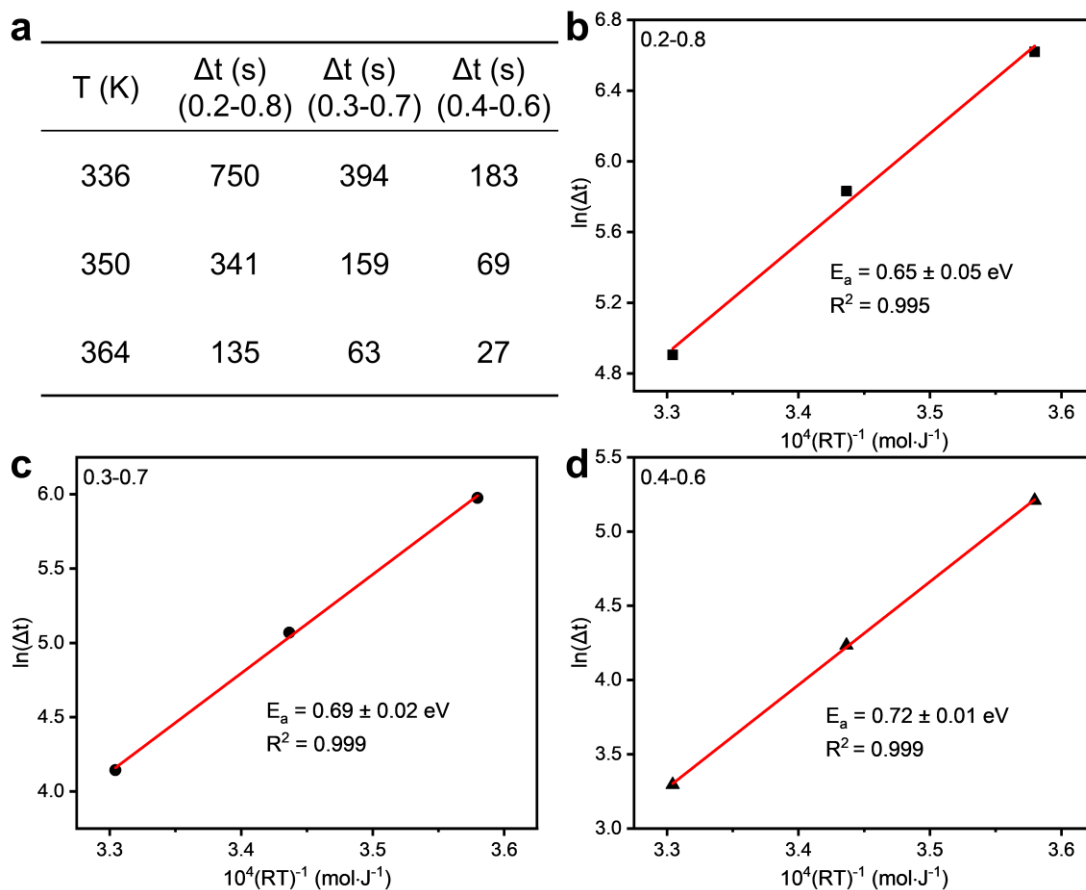
The normalized brightness value (I_B) in this work was acquired using the equation:

$$I_B = \frac{I - I_{min}}{I_{max} - I_{min}} \tag{1}$$

where, I is the integrated area beneath the brightness profile, as shown in (b). I_{max} and I_{min} are the maximum and minimum values of I, respectively.

In light of this, the normalized darkness value (I_D) is defined by equation (2):

$$I_D = 1 - I_B \tag{2}$$

a

T (K)	Δt (s) (0.2-0.8)	Δt (s) (0.3-0.7)	Δt (s) (0.4-0.6)
336	750	394	183
350	341	159	69
364	135	63	27

Fig. S8 (a) The data table showing the interval of time (Δt) corresponding to different stages of transformation during the decolorization process (The brightness increased from 0.2 to 0.8, from 0.3 to 0.7, and from 0.4 to 0.6, respectively.) and the corresponding decolorization temperature. (b,c,d) The activation energy (E_a) of thermal decoloration can be determined from the slope of the fitting straight line obtained by plotting ln(Δt) versus 1/RT.
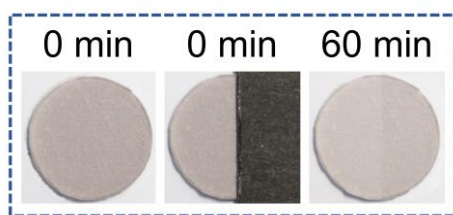
Fig. S9 The photograph of a LiCaPO$_4$:0.5%Gd^{3+} phosphor disc recorded immediately after 20 min of X-ray irradiation and comparison of the left side (after decolorizing for 1 h in an indoor light environment (50 lux) at room temperature) and the right side (after bleaching for 1 h in dark at room temperature) of the LiCaPO$_4$:0.5%Gd^{3+} phosphor disc.
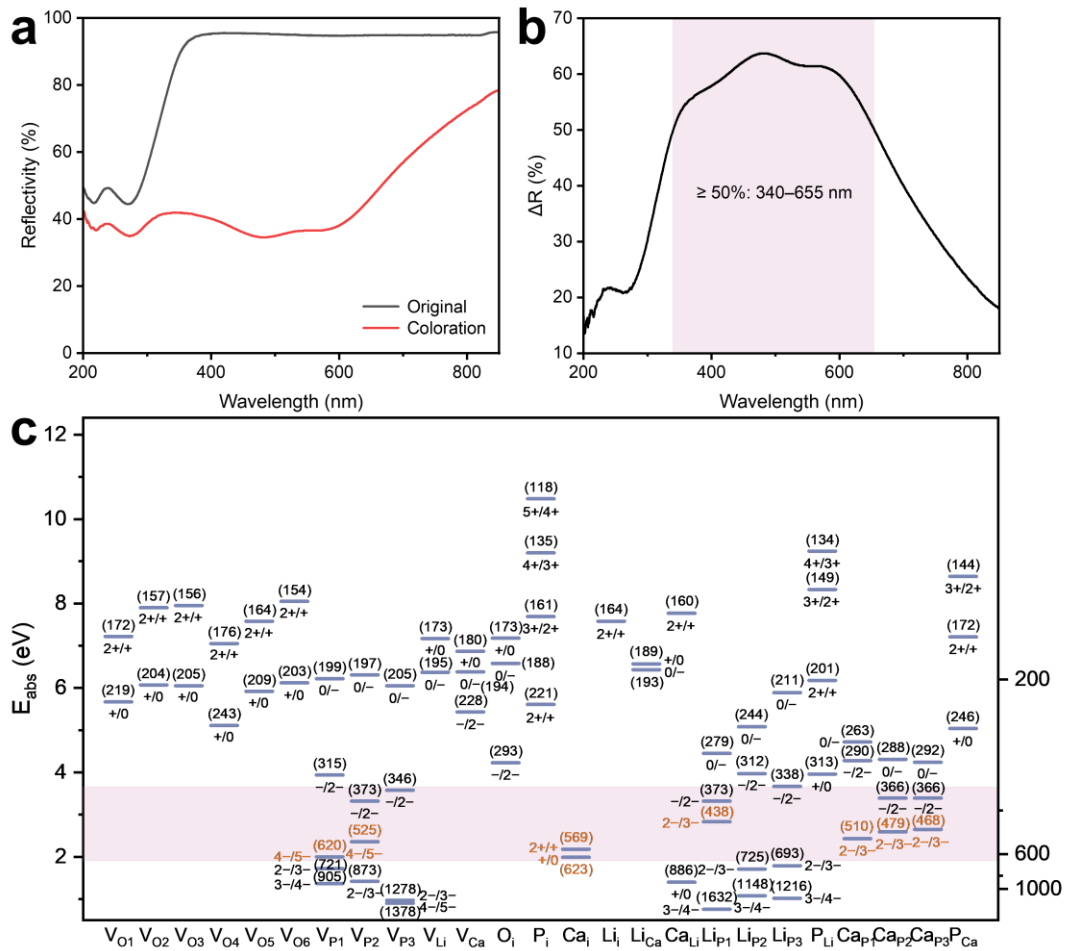
Fig. S10 (a) Diffuse reflectance spectra of the LiCaPO$_4$:0.5%Gd^{3+} phosphor before and after X-ray irradiation. (b) Variation in the reflectance (ΔR) of the LiCaPO$_4$:0.5%Gd^{3+} phosphor at various wavelengths after X-ray irradiation. (c) Calculated absorption energies and wavelengths for excitons trapped at intrinsic point defects in LiCaPO$_4$. The values in parentheses (in nm) show the corresponding absorption wavelengths.

Table S1 NB-UVB persistent luminescence power intensities measured by the power meter.

Decay time (s)	Irradiance (mW·m^{-2})
30	11.79
60	9.21
90	7.77
120	6.80
150	6.08
300	4.28
600	2.83
900	2.07